Materials Advances

ROYAL SOCIETY OF CHEMISTRY

PAPER

View Article Online
View Journal | View Issue

Check for updates

Cite this: *Mater. Adv.*, 2026, 7, 3736

Additive manufacturing of semiconductive polymer nanocomposites loaded with tungsten disulfide nanosheets

Luisa M. Valencia Liñán, † Alberto Sanz de León, * Sergio I. Molina and Miriam Herrera

In this work, we report the development of novel tungsten disulfide nanocomposites with optical and electrical properties suitable for stereolithography (SL). The dispersion of WS_2 nanosheets (WS_2-2D) after exfoliation *via* liquid-phase in DMF could be directly incorporated into commercial photopolymer resins, which allowed the successful printing of WS_2-2D nanocomposites with different degrees of complexity. The manufactured nanocomposites, with measured WS_2-2D ultra-low concentrations in the range of 0.001 to 0.005 wt%, imparted a green coloration and red fluorescence to the printed parts while maintaining their transparency due to the nanometric size and good exfoliation of the filler. Interestingly, the electrical resistivity of the nanocomposites decreased by eight orders of magnitude compared to the pristine resin, reaching values in the semiconductive range. These findings highlight the potential of WS_2-2D nanocomposites for the additive manufacturing of functional components with applications in areas such as plasmonic, photonics, and electronics.

Received 29th January 2026,
Accepted 5th March 2026

DOI: 10.1039/d6ma00134c

rsc.li/materials-advances

Open Access Article. Published on 06 March 2026. Downloaded on 5/24/2026 12:24:54 AM.
This article is licensed under a Creative Commons Attribution-NonCommercial 3.0 Unported Licence.

Introduction

Over the past decade, two-dimensional (2D) materials have attracted renewed attention due to their exceptional properties derived from their ultrafine atomic structure. Although graphene pioneered this field and remains the most studied thanks to its high electrical conductivity, mechanical strength, and flexibility, other 2D materials have since emerged, offering complementary features that expand the range of potential applications.[1] Among these, transition metal dichalcogenides (TMDs), MX_2-type compounds consisting of hexagonal layers of transition metal atoms (M), such as tungsten or molybdenum, sandwiched between two layers of chalcogen atoms (X), such as sulfur, selenium, or tellurium, stand out for their semiconducting, plasmonic, photonic, and catalytic properties.[2,3] Unlike graphene, many TMDs exhibit a transition from an indirect band gap in their bulk form to a direct band gap when thinned down to monolayers, significantly enhancing their efficiency in light absorption and emission. This makes monolayer TMDs ideal candidates for optoelectronic devices, high-efficiency transistors, chemical sensors, and electrochemical catalysis.[4–7] Tungsten disulfide (WS_2) is particularly promising due to its chemical stability, high charge carrier mobility, and strong light-matter interactions, positioning it as a key material in emerging fields such as flexible nanoelectronics and photonics.[8–10]

In addition to its conventional electronic and optical properties, WS_2 nanosheets (WS_2-2D) exhibits notable plasmonic properties when arranged in nanoscale structures. These plasmonic effects arise from the collective resonance of free electrons induced by the light interaction, enabling WS_2 to manipulate light at subwavelength scales. This facilitates optical signals amplification and improves efficiency in photonic and optoelectronic applications.[11,12] Exploiting these properties brings new opportunities for the development of ultrasensitive sensors, integrated photonic devices, and materials with selective light absorption capabilities, aspects that are particularly relevant in the engineering of functional nanocomposites.

Beyond its use in electronics and photonics, the incorporation of WS_2-2D into polymer matrices for the manufacture of nanocomposites has emerged as a promising approach to enhance the functional properties of conventional polymers. The addition of 2D nanomaterials can confer novel functionalities thereby expanding the range of possible applications.[13–15] Within this context, additive manufacturing (AM) and, more specifically, photopolymerization-based 3D printing techniques like stereolithography (SL), has become an advanced method that enables the rapid and precise fabrication of complex parts with high surface resolution.[16–18] The basic principle of the

Dpto. Ciencia de los Materiales, I. M. y Q. I., IMEYMAT, Facultad de Ciencias, Universidad de Cádiz, Campus Río San Pedro, s/n, 11510 Puerto Real (Cádiz), Spain. E-mail: alberto.sanzdeleon@uca.es

† Current address: Instituto de Ciencia de Materiales de Sevilla (CSIC-US), Americo Vespucio 49, Seville 41092, Spain.

© 2026 The Author(s). Published by the Royal Society of Chemistry

Open Access Article. Published on 06 March 2026. Downloaded on 5/24/2026 12:24:54 AM. This article is licensed under a Creative Commons Attribution-NonCommercial 3.0 Unported Licence.

process is to solidify a photocurable resin by using a UV laser source to build up the entire object layer by layer.

Despite their advantages, conventional resins for SL typically exhibit limited damage tolerance and intrinsically insulating behavior, which together constrain their use in structurally demanding or functional components. In this context, polymer nanocomposites incorporating functional fillers have emerged as a promising route to overcome these limitations and endow 3D-printed parts with enhanced mechanical performance and tailored electrical properties.[19–21] Therefore, the incorporation of nanomaterials, such as WS_2-2D, into these resins offers a pathway to develop nanocomposites with improved structural and functional properties. Tal *et al.*[22] reported the incorporation of WS_2-2D into acrylate resins for SL, showing enhanced photopolymerization rates and significant mechanical reinforcement of the printed parts, thus evidencing the suitability of these nanomaterials as additives in photocurable systems. However, their work was limited to structural aspects (curing kinetics and mechanical performance) and did not explore potential optoelectronic functionalities. However, the optical and electronic capabilities of WS_2-2D have been widely demonstrated in composites fabricated by other processing routes, where they have attracted considerable interest for optoelectronic applications.[23–25] Despite this, studies addressing the integration of WS_2-2D into SL resins remain scarce, highlighting the need for optimized dispersion approaches and systematic evaluation of functional properties in WS_2-based SL nanocomposites.

Building on this gap, we propose in the present paper a method to fabricate WS_2-2D nanocomposites with enhanced optical and electrical properties, using SL Specifically, we investigate the role of DMF in the liquid-phase exfoliation of commercial WS_2 at different concentrations and compare it with direct exfoliation within the SL acrylic resin. This approach allows us to assess how WS_2-2D concentration, dispersion quality, and solvent presence influence both the printing process and the resulting functional performance. Notably, the incorporation of WS_2-2D enables tunable electrical resistivity (down to 10^7 Ω cm) together with photoluminescent behavior in the printed parts, thereby addressing a current gap in the development of functional 3D-printed nanocomposites.

Materials and methods

Materials

WS_2 microparticles were purchased from Sigma-Aldrich. Dimethylformamide (DMF) was purchased from Scharlab. Clear standard photopolymer resin for vat photopolymerization was purchased from XYZprinting.

WS_2 exfoliation

A VWR Ultrasonic Cleaner USC500T working at 45 kHz was used to exfoliate WS_2 into 2D nanosheets. Different WS_2 concentrations in DMF between 1 and 50 mg mL^{-1} were tested and sonication times ranged from 0.5 to 24 h. An intense dark green color evidences the success of the exfoliation. The water of the ultrasonic bath was replaced regularly (typically each 30 min) to ensure that its temperature was always below 25 °C. Then, the dispersion was centrifuged for 30 min at 6000 rpm to separate the exfoliated WS_2 nanosheets (WS_2-2D) from the bulk WS_2, keeping the supernatant solution and discarding the solid content at the bottom of the tubes.

3D-printing of WS_2 nanocomposites

The WS_2-2D composites were manufactured in a Nobel 1.0 SL 3D-printer (XYZPrinting). Ratios of 1 : 9, 1 : 4, 1 : 3 and 1 : 2 of WS_2-2D dispersed in DMF and resin were tested, leading to resins named R1, R2, R3 and R4, respectively. A control in absence of WS_2-2D (R0) was also printed. The actual concentration of WS_2-2D in the resin was calculated by UV-Vis, measuring the absorbance value of the exciton at 632 nm.[26] Then, different objects, including electrical conductivity discs according to ASTM D257 standard, 100 μm-thick films and complex structures that cannot be manufactured by classical techniques were printed. All the printed objects were then post-processed in a Formlabs FormCure chamber equipped with a light source of 405 nm and a power of 1.25 mW cm^{-2} for 60 min at room temperature to ensure full polymerization of the resin.

Characterization

UV–Vis analyses were carried out in a Varian Cary 50 Conc spectrophotometer. The viscosity of the resins was measured using a Rotavisc lo-vi (IKA) equipped with a SP-1 spindle. Measurements were carried out at 25 °C using a shear rate of 1 s^{-1}. Fourier-transform infrared spectroscopy in attenuated total reflectance mode (FTIR-ATR) was performed between 4000 and 650 cm^{-1} (32 scans, 4 cm^{-1} resolution) using a Bruker Alpha spectrometer. Thermogravimetric analysis (TGA) was performed using a TA Instruments Q50 from 25 °C to 600 °C at 10 °C min^{-1} under air atmosphere. Scanning electron microscopy (SEM) measurements were performed on Au-coated specimens (5 nm coating thickness) using a FEI Nova NanoSEM 450 microscope equipped with a field-emission gun and provided with a concentric annular detector suitable for compositional backscattering (CBS) electron imaging displaying Z-contrast. Transmission electron microscopy (TEM) was performed in a FEI Talos F200X operated at 200 kV. The microscope is equipped with a Schottky field emission gun (XFEG) and a ChemiSTEM EDX detector, providing high-resolution and high angle annular dark-field (HAADF) TEM imaging and spectroscopic measurements (energy dispersive X ray spectroscopy (EDX)). The electron-transparent specimens for TEM analyses were obtained by ultramicrotomy. The samples were sectioned into thin slices using a Leica EM UC7 ultramicrotome equipped with a diamond knife working at room temperature. After cutting, the sections were deposited on 300 mesh Cu grids. Fluorescence spectroscopy and imaging was done using a Zeiss Axio Observer Z1 inverted fluorescence optical microscope equipped with a LSM880 confocal laser scanning system and a Fast AiryScan high-speed super-resolution module. Fluorescence spectra were obtained from

Open Access Article. Published on 06 March 2026. Downloaded on 5/24/2026 12:24:54 AM.
This article is licensed under a Creative Commons Attribution-NonCommercial 3.0 Unported Licence.

areas of 90 μm^2 and images were recorded at the same exposure conditions so they can be directly compared. Electrical conductivity was measured according to ASTM D257 in a Keithley 6517B electrometer applying a voltage of 500 V. In all cases, three different specimens of each nanocomposite were tested, and the results are reported as mean values, with the error corresponding to the standard deviation.

Results and discussion

A first attempt to prepare polymer nanocomposites loaded with WS_2-2D was carried out by dispersing bulk WS_2 in a photocurable resin for SL under sonication at different times. Although various studies have shown that WS_2 can be exfoliated mechanically *via* ultrasonication in suitable solvents, there are no reports on its exfoliation in viscous media such as resin precursors.

Fig. 1 shows the evolution of the absorbance of the WS_2-resin dispersion. Initially, a high absorbance is observed around 400 nm, mainly due to the resin itself. As sonication time increases, the absorbance across the entire visible spectrum gradually rises, as expected, due to the scattering of large, micron-sized WS_2 particles. After 4 h of sonication, the spectra become noticeably noisier, indicating increased light scattering caused by the presence of smaller but not fully exfoliated, micron-sized WS_2 particles. Since these particles are smaller, their sedimentation time is higher, leading to noisier spectra because of a higher amount of scattered light. This suggests that while ultrasonication improves the homogeneity of the dispersion and prevents sedimentation, it is insufficient for producing well-exfoliated WS_2-2D nanosheets.

Interestingly, after 24 h of sonication, a weak absorption band appears at *ca.* 630 nm, which can be assigned to the A excitonic transition of WS_2-2D.[27] Despite the significant background noise due to scattering, this feature confirms the partial formation of 2D nanomaterials. However, attempts to separate these exfoliated nanosheets from the remaining larger particles by centrifugation were unsuccessful, likely due to the high viscosity of the resin.

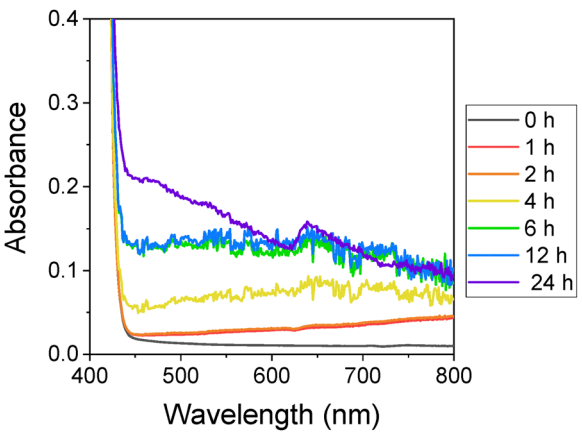

Fig. 1 UV-vis spectra of 3 mg mL^{-1} WS_2 dispersed in the photopolymer resin after sonication at different times.

Therefore, while this simple method demonstrates a degree of exfoliation, it is not practical for large-scale or consistent production. The long sonication times required and the limited yield of nanosheets make it inefficient. This limitation is likely related to the relatively high viscosity of the resin (1180 ± 120 mPa s), which hinders the exfoliation process, similar to what has been observed in other similar systems.[28,29]

As an alternative approach, WS_2 exfoliation *via* ultrasonication in DMF was further explored. The exfoliation in organic solvents is well-documented,[30] with several studies highlighting the importance of solvent selection and concentration. In this work, our objective is to maximize the overall content of exfoliated WS_2 rather than to selectively isolate monolayers. Consequently, the term WS_2-2D is used throughout the manuscript to describe the entire population of WS_2 nanomaterials, including both single-layer and few-layer nanosheets. This terminology reflects the intrinsic statistical nature of liquid-phase exfoliation, where achieving complete monolayer selectivity is inherently challenging.[31] Considering this, an initial experiment was conducted using a fixed WS_2 concentration of 10 mg mL^{-1} to determine the optimal sonication time.

Fig. 2(a) shows the evolution of the WS_2 absorption spectra with increasing sonication time. In all cases, a main band is observed at around 632 nm and a weaker band at approximately 520 nm, ascribed to the so-called A and B excitons, respectively. These bands can be ascribed to the electronic transitions, characteristics of WS_2-2D.[27] For clarity, Fig. 2(b) plots the intensity of the A exciton peak as a function of sonication time, clearly illustrating that exfoliation improves up to 3 h, after which the WS_2-2D content begins to decrease. Sonication beyond 4.5 h did not further enhance exfoliation. This decline may be attributed to the restacking of WS_2-2D nanosheets during prolonged ultrasonication into larger, micron-sized aggregates, as suggested by other studies.[32]

When these results are compared to those from Fig. 1, it becomes evident that DMF is significantly more effective than the resin medium, achieving higher exfoliation yields in much shorter times. For example, after 180 min, the absorbance in DMF reaches values of 0.4–0.5, whereas in the resin, the maximum absorbance after 24 h remains below 0.2. Furthermore, the spectra recorded in DMF are markedly clearer, owing to the successful separation of WS_2-2D from bulk WS_2 *via* centrifugation.

Next, a screening was performed using different WS_2 concentrations ranging from 1 to 50 mg mL^{-1}, with the exfoliation time fixed at 3 h. As shown in Fig. 3, DMF maintained relatively stable absorbance values, between 0.4 and 0.6, even at concentrations up to 30 mg mL^{-1}, indicating good exfoliation stability under these conditions, thus making DMF a suitable solvent as the exfoliation medium for concentrations up to 30 mg mL^{-1}. To isolate WS_2 nanosheets from larger particulate residues, the dispersions were centrifuged at 6000 rpm for 30 min. The lateral dimensions of the resulting WS_2-2D nanosheets were characterized by high-resolution SEM imaging. As shown in Fig. 4, these conditions yielded nanosheets with a relatively narrow size distribution and a pronounced tendency toward

© 2026 The Author(s). Published by the Royal Society of Chemistry

Open Access Article. Published on 06 March 2026. Downloaded on 5/24/2026 12:24:54 AM.
This article is licensed under a Creative Commons Attribution-NonCommercial 3.0 Unported Licence.

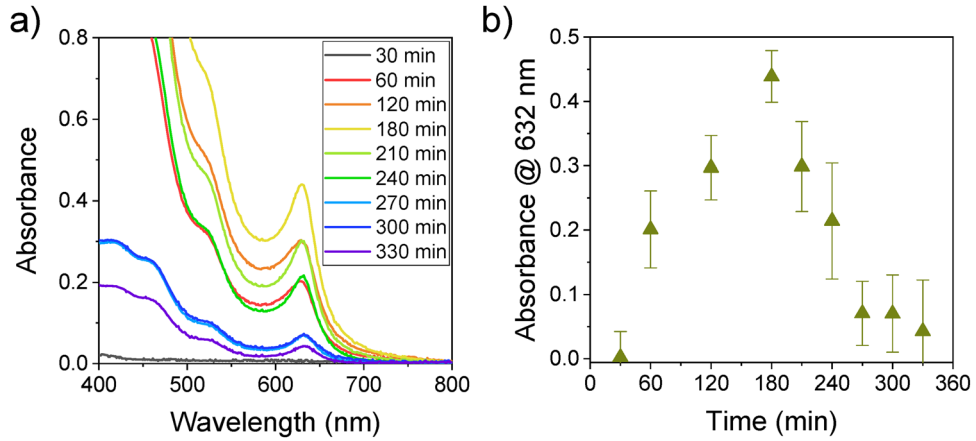

Fig. 2 (a) UV-vis spectra of 10 mg mL^{-1} WS_2 dispersed in DMF after sonication at different times; (b) evolution of WS_2-2D absorbance with time, recorded at 632 nm.

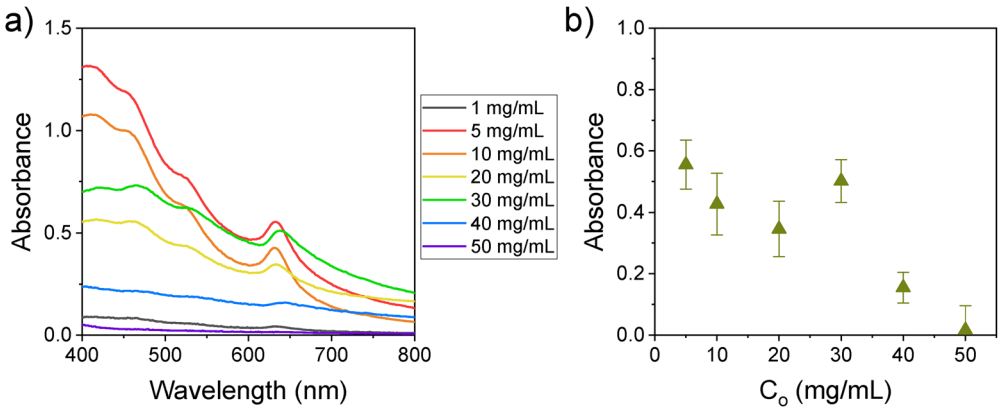

Fig. 3 (a) UV-vis spectra of WS_2 dispersed at different concentrations in DMF after 180 min of sonication; (b) evolution of the absorbance of WS_2-2D, measured at λ = 632 nm.

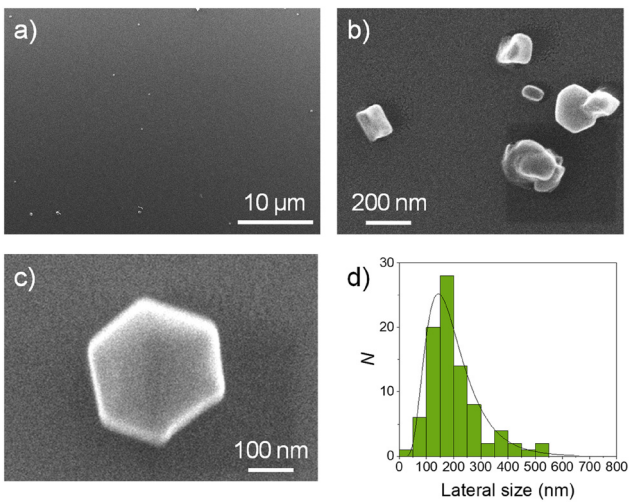

Fig. 4 (a–c) SEM images and (d) size distribution of the WS_2-2D dispersed in DMF after 180 min of sonication and separation by centrifugation at 6000 rpm.

hexagonal geometry. Statistical analysis of the SEM measurements reveals that the lateral size distribution is well described by a lognormal function, providing an excellent fit to the experimental data. The fitted distribution yields a median lateral size of 170 nm, with D_{10} and D_{90} values of about 95 nm and 310 nm, respectively.

Then, attempts were made to concentrate the exfoliated nanosheets *via* centrifugation and vacuum distillation after exfoliation in DMF to maximize the amount of WS_2-2D in the nanocomposites. However, this approach proved unsuccessful. On one hand, the high boiling point of DMF (153 °C) makes solvent removal highly energy-intensive. Furthermore, during distillation, the dispersions gradually lose their characteristic green color (typically associated with WS_2-2D) and turn dark, indicating the restacking of nanosheets into bulk WS_2. This phenomenon is likely driven by the combined effects of elevated temperature and increasing local WS_2 concentration during solvent evaporation.

Despite this limitation, previous studies have demonstrated that the presence of DMF does not interfere with the

Open Access Article. Published on 06 March 2026. Downloaded on 5/24/2026 12:24:54 AM.
This article is licensed under a Creative Commons Attribution-NonCommercial 3.0 Unported Licence.

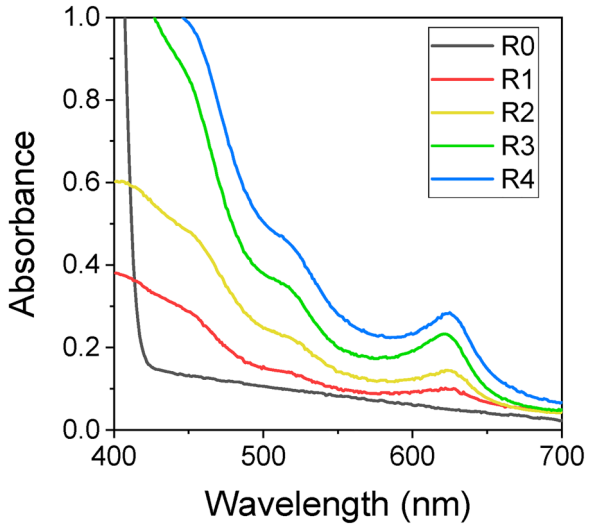

Fig. 5 UV-vis spectra of the WS_2-2D nanocomposites.

photopolymerization process of stereolithography resins.[33] Therefore, although the use of DMF restricts the maximum amount of WS_2-2D that can be incorporated, the WS_2-2D dispersions in DMF were directly mixed with a commercial photopolymer resin in different proportions to formulate printable nanocomposites. Based on this approach, a series of resin precursors was prepared using DMF : resin volume ratios of 1 : 9, 1 : 4, 1 : 3, and 1 : 2, denoted as R1, R2, R3, and R4, respectively. A neat resin without WS_2-2D was also prepared as a control (R0). As batch-to-batch variations in the concentration of WS_2-2D dispersed in DMF may occur, their actual content in each formulation (after mixing with the resin) was determined by UV-vis spectroscopy (Fig. 5). For this, a molar extinction coefficient of 615 mL mg^{-1} m^{-1} was used for the A exciton of the WS_2-2D, as reported in the literature.[26] The resulting WS_2-2D concentrations in the resins, summarized in Table 1, range from 0.001 to 0.005 wt%. The viscosity of all resin formulations was also measured to ensure printability by SL, for which viscosities typically in the range of 100–10 000 mPa s are considered optimal.[34] Formulations R1, R2, and R3 exhibit viscosities within this acceptable window, as shown in Table 1. In contrast, R4 displays a markedly reduced average viscosity of 38 mPa s, nominally below the usual recommendation. Nevertheless, under our printing conditions, R4 could still be printed reproducibly without visible phase separation or loss of dimensional fidelity. This is consistent with reports demonstrating successful printing of low-viscosity resins with values as low as 20 mPa s, particularly when short recoating distances and moderate speeds that minimize over-spreading.[34,35] Further increasing the DMF content led to unstable layer leveling and occasional print failures, so no higher DMF fractions were pursued, and the maximum practical WS_2-2D loading for this approach was established at 0.005 wt%.

Then, all nanocomposite formulations were successfully printed *via* SL using the standard laser power and scanning speed settings optimized for the commercial resin. Notably,

Table 1 Formulation parameters and properties of the resins used in this study, including DMF : resin ratio, A-exciton absorbance, WS_2-2D concentration, and viscosity measured at 1 s^{-1}

Name	DMF : resin ratio	A-exciton absorbance	WS_2-2D conc. (wt%)	Viscosity (mPa s)
R0	0	0.101	0	1180 ± 120
R1	1 : 9	0.144	0.001	464 ± 21
R2	1 : 4	0.232	0.002	241 ± 23
R3	1 : 3	0.284	0.003	110 ± 4
R4	1 : 2	0.412	0.005	38 ± 6

even formulation R4, despite its unexpectedly low viscosity, could be printed without observable defects. Although DMF was included in the formulation to stabilize the dispersion of WS_2-2D, its presence in the final printed structures appears to be negligible. It must be noted that, after post-curing, the printed parts are fully solid and do not exhibit any visible signs of residual solvent (swelling, tackiness or softening), suggesting that most of the DMF added for WS_2 exfoliation is not present in the nanocomposite after the layer-by-layer photopolymerization and subsequent post-curing. In this scenario, we hypothesize that the photocuring process would effectively trap the WS_2-2D nanosheets within the three-dimensional polymer network, while DMF diffuses out of the forming solid. Similar behavior was also observed in our previous work involving silver nanocomposites for SL, where the presence of DMF did not compromise print quality.[33] To confirm this, TGA analysis was performed. Fig. 6(a) shows that the curves for R0 (without DMF) and R4 (highest content of DMF in the formulation) are practically identical. A magnified view of the region around 153 °C (*i.e.* the boiling point of DMF) reveals only a very small difference, with R4 exhibiting a slightly lower mass than R0. However, this difference is below 0.7%, indicating that any DMF remaining trapped in the resin is minimal. This conclusion is further supported by FTIR-ATR (Fig. 6(b)), where the spectra of R1–R4 nanocomposites are nearly identical to that of the pristine resin R0 and the characteristic DMF absorption bands (C=O stretching at 1670 cm^{-1} and C–N stretching at 1502 cm^{-1}) are not detected in any case.[36]

Fig. 7 presents several examples of printed objects. As shown in Fig. 7(a), increasing WS_2-2D concentration leads to a visibly greener and darker appearance, confirming the presence of nanosheets. Despite the coloration, the objects remain optically transparent since the dimensions of the nanosheets are well below the diffraction limit of visible light. Additionally, as shown in Fig. 7(b), complex geometries, unachievable *via* conventional techniques such as injection molding, were successfully printed with dimensional accuracy within standard SL tolerances (±0.1–0.2 mm), demonstrating that neither the presence of WS_2-2D nor DMF significantly impairs the photopolymerization of the resin. The results obtained confirm the feasibility of printing WS_2-2D nanocomposites using DMF as a dispersing medium.

The surface morphology of the R2 nanocomposite was examined by SEM (Fig. 8(a–c)) to gain insight into its microstructure. Although some features can be observed in the

© 2026 The Author(s). Published by the Royal Society of Chemistry

Open Access Article. Published on 06 March 2026. Downloaded on 5/24/2026 12:24:54 AM.
This article is licensed under a Creative Commons Attribution-NonCommercial 3.0 Unported Licence.

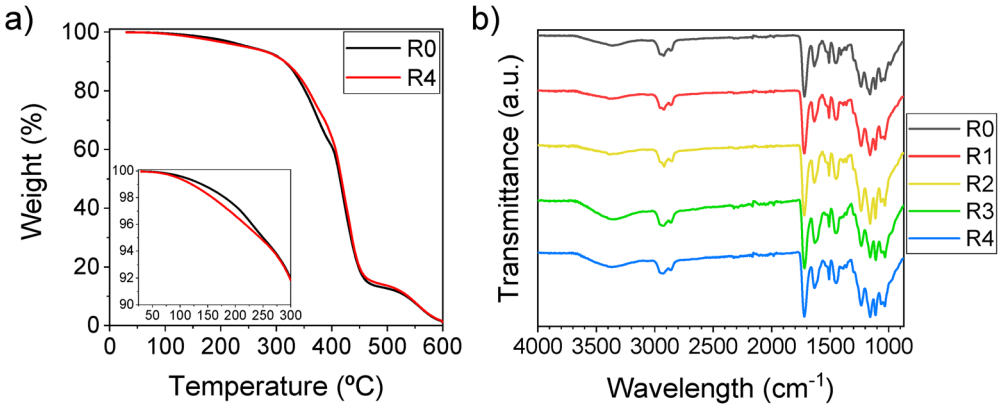

Fig. 6 (a) TGA thermograms of R0 and R4; (b) FTIR spectra of the WS_2-2D nanocomposites.

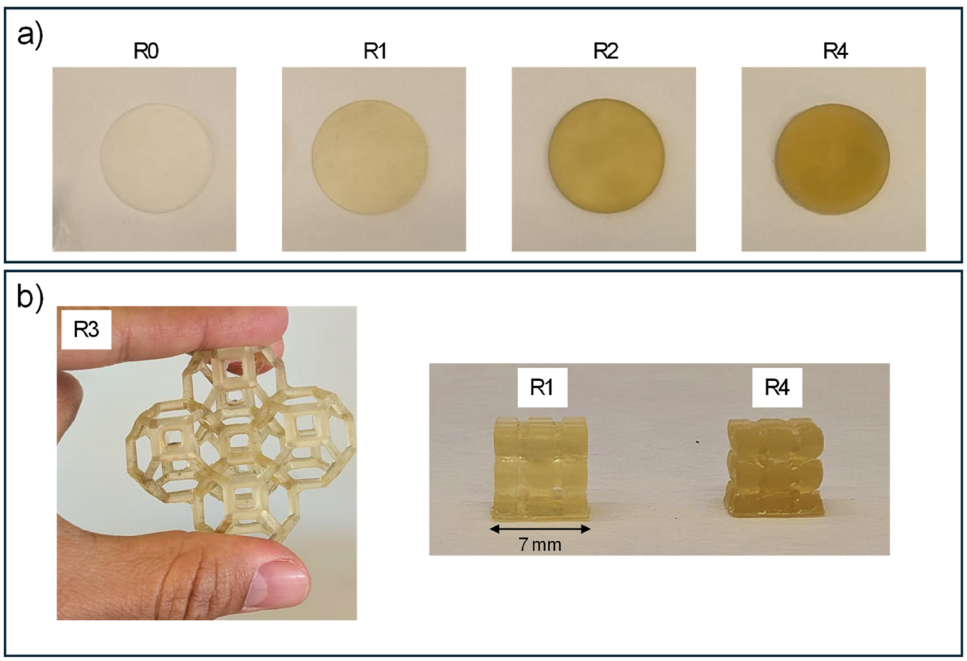

Fig. 7 Digital pictures of (a) electrical conductivity discs prepared with different amounts of WS_2-2D; and (b) complex objects with cavities and hollow structures that cannot be printed by classic manufacturing techniques.

SEM images that exhibit a morphology like that of WS_2-2D nanosheets dispersed in DMF, their presence cannot be unambiguously identified using this technique. This limitation arises primarily from the intrinsic surface roughness of the printed composites, which makes it difficult to distinguish WS_2-2D nanosheets from the background roughness of the polymer matrix, as previously reported.[37] In addition, the very small lateral dimensions of the nanosheets and their low concentration within the resin further hinder their reliable detection by SEM when they are embedded in the resin. Attempts to obtain compositional information from the SEM images by EDX analysis were also unsuccessful, mainly because any signal potentially generated by the WS_2-2D nanosheets is too weak to be detected, due to their small size and low concentration.

For this reason, the composites were further investigated by TEM. Electron-transparent lamellae were prepared from the nanocomposites by ultramicrotomy and subsequently analyzed by TEM. Fig. 8(d and e) show HAADF-TEM images in which nanosheets can be clearly observed as regions with higher contrast than the polymer matrix. This contrast originates from the Z-dependent nature of HAADF imaging, where heavier elements (W and S in WS_2-2D) produce stronger signals than lighter elements (such as C in the resin). As a result, the WS_2-2D can be directly visualized within the composite, confirming that they retain their nanosheet morphology. Complementary TEM–EDX analysis (Fig. 9) further confirmed that these nanostructures correspond to WS_2-2D.

Then, the optical properties of the WS_2-2D nanocomposites were investigated by fluorescence microscopy. To this end, the

Open Access Article. Published on 06 March 2026. Downloaded on 5/24/2026 12:24:54 AM.
This article is licensed under a Creative Commons Attribution-NonCommercial 3.0 Unported Licence.

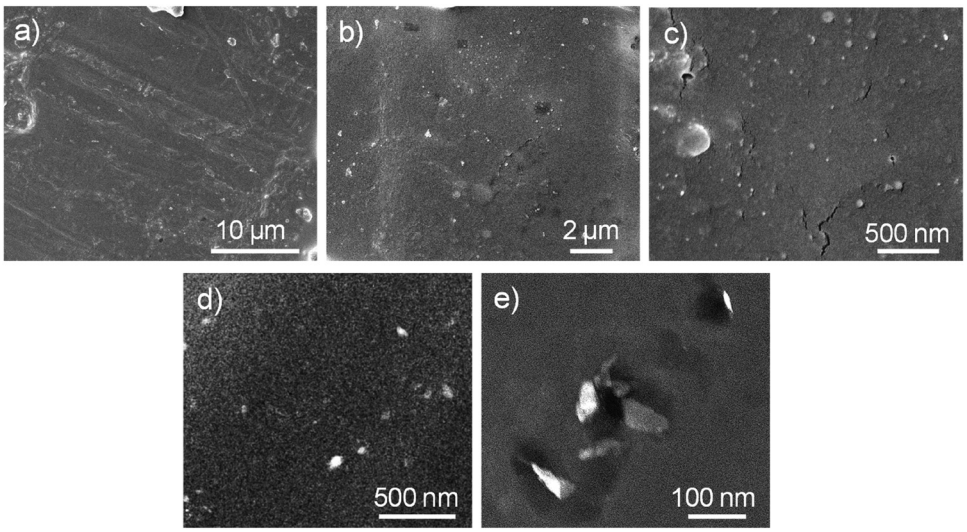

Fig. 8 (a)–(c) SEM and (d)–(e) TEM micrographs of R2 nanocomposite.

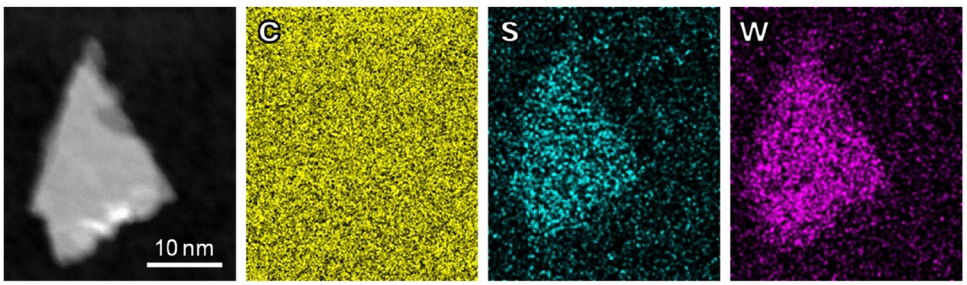

Fig. 9 TEM-EDX analysis of one WS_2-2D nanosheet embedded in R2 nanocomposite. Left panel corresponds to HAADF-TEM signal, while images in yellow, cyan and magenta correspond to the EDX signals of C, S and W, respectively.

emission under different excitation wavelengths was first evaluated using a single 100 μm-thick 3D-printed layer of the R4 nanocomposite. No emission was detected in the visible region (up to 800 nm) under 632 nm excitation, where the A exciton was previously observed. However, red fluorescence was observed when R4 was excited at 520 nm, where the band corresponding to the B exciton is located (see Fig. 5). In this case, the material exhibited light emission with a maximum near 620 nm. The intensity of this fluorescence varied when other wavelengths around 520 nm were tested, reaching a maximum at 560 nm (Fig. 10(a)). This trend aligns with previous studies indicating that red fluorescence is typically only observed in monolayer or few-layer WS_2, as thicker particles show reduced emission in the visible region.[38] These findings support that most WS_2 in the nanocomposite is present as exfoliated monolayers or few-layer nanosheets. The observed fluorescence thus provides indirect but strong evidence of successful exfoliation and incorporation of WS_2-2D into the resin. Both absorption and emission bands are slightly red-shifted with respect to typical values reported for WS_2 flakes deposited on rigid, low-index substrates. This shift can be attributed to a combination of environmental effects: the higher refractive index (n = 1.527) and dielectric screening of the crosslinked resin compared to air or aqueous media, possible interfacial charge-transfer interactions between WS_2-2D and the polymer, and local strain or nanosheet aggregation within the polymer network. Similar red-shifts and lineshape modifications of photoluminescence have been reported upon embedding liquid-exfoliated WS_2-2D in polymer matrices or upon changing the dielectric environment and substrate, highlighting the strong sensitivity of excitonic transitions in WS_2-2D to their surroundings.[39,40] To our knowledge, this is the first report of such emission from printable WS_2-2D nanocomposites prepared by SL. A similar effect was also observed in our previous studies of gold-based printable nanocomposites,[41] highlighting the potential of these materials for tunable plasmonic applications.

Fig. 10(b) presents fluorescence optical microscopy images of the R4 nanocomposite. Different regions of the sample exhibit clear red fluorescence; however, individual WS_2-2D nanosheets cannot be resolved. This indicates that the nanosheets are below the optical diffraction limit of the microscope and suggests the absence of significant aggregation within the resin after printing. For comparison, a control sample containing a similar concentration of unexfoliated WS_2 was also examined under identical exposure conditions,

 © 2026 The Author(s). Published by the Royal Society of Chemistry

Open Access Article. Published on 06 March 2026. Downloaded on 5/24/2026 12:24:54 AM.
This article is licensed under a Creative Commons Attribution-NonCommercial 3.0 Unported Licence.

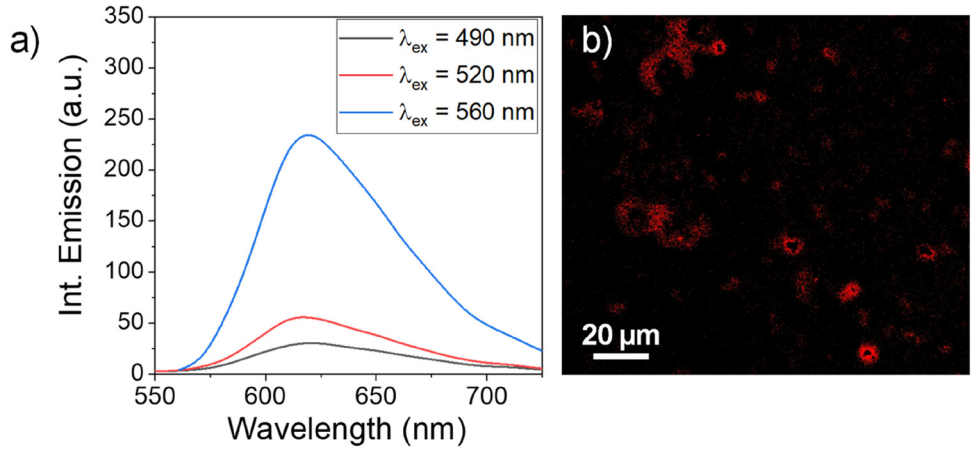

Fig. 10 (a) Emission spectra recorded upon excitation at different wavelengths and (b) fluorescence microscopy image upon excitation at 560 nm of one R4 100 µm-thick film.

but no fluorescence signal was detected, in agreement with previous studies.[38,42] This comparison highlights the critical role of exfoliation in preserving the optical activity of WS_2 and confirms that the WS_2-2D nanosheets retain their optical functionality after stereolithographic (SL) processing. Overall, these results demonstrate that WS_2-2D nanosheets are successfully exfoliated, homogeneously dispersed, and retained within the printed resin, while preserving their intrinsic optical properties after printing. This makes them promising candidates for integration into optoelectronic and photonic polymer-based materials.

Finally, the electrical properties of the nanocomposites were evaluated. Fig. 11 shows the electrical resistivity of the different nanocomposites printed. The results indicate that increasing the WS_2-2D content leads to a significant decrease in resistivity, where even R1 makes the resistivity decrease by six orders of magnitude. As the WS_2 concentration increases, resistivity values continue to drop, reaching values in the range of 10^7 Ohm cm, which lies within the range of semiconductive materials. Although trace amounts of residual DMF may remain in the nanocomposites after printing, control experiments from our previous work showed that this decreases the resistivity by only one order of magnitude.[33] Similarly, nanocomposites with non-exfoliated WS_2 exhibited resistivities around 10^{15} Ohm cm, confirming that the dramatic reduction in WS_2-2D nanocomposites arises primarily from successful exfoliation. This behavior may be attributed to variable range hopping mediated by electron tunneling between isolated WS_2-2D nanosheets, facilitated by their high aspect ratio, edge states, and intrinsic semiconductivity.[43] At low loadings (below 0.005 wt%), classical 3D percolation is implausible, but 2D fillers could enable transient conductive paths *via* quantum tunneling across thin insulating gaps, as previously shown for graphene and other TMD nanocomposites.[44–46] This behavior makes these materials promising for ESD applications as protective components, particularly in customized or complex geometries where conventional manufacturing techniques are limited, as well as in electronic devices for plasmonic and photonic applications.

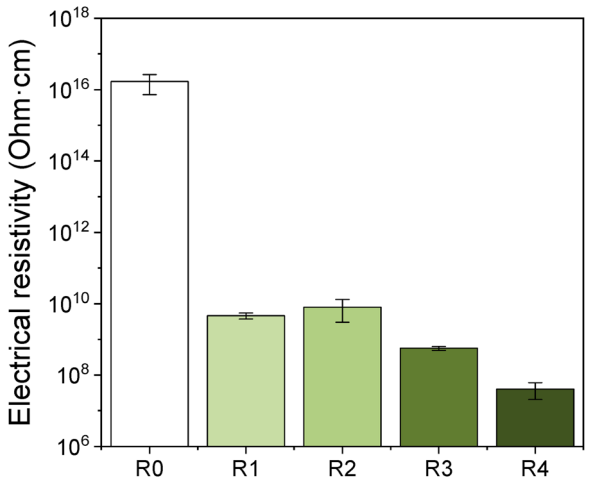

Fig. 11 Electrical resistivity of the WS_2-2D nanocomposites.

Conclusions

In this work, we have developed a series of WS_2-based nanocomposites with tunable optical and electrical properties, suitable for 3D printing *via* SL. WS_2-2D nanosheets were successfully obtained *via* ultrasound-assisted liquid-phase exfoliation in DMF. The resulting dispersions were directly incorporated into commercial resin formulations without compromising printability, enabling the fabrication of WS_2-2D nanocomposites. Spectroscopy and microscopy analysis revealed that the WS_2-2D enabled the production of translucent, green-colored printed parts that exhibited red fluorescence. This emission, red-shifted relative to previous reports on WS_2-2D in solution, demonstrates the potential of these nanocomposites due to the embedding of WS_2-2D within the polymer matrix. Additionally, the use of WS_2-2D resulted in a more homogeneous dispersion of the nanofillers, which facilitates electron transport across the polymer matrix. As a result, a dramatic reduction in electrical resistivity (down to 10^7 Ohm cm) was achieved at unprecedentedly low WS_2-2D

Open Access Article. Published on 06 March 2026. Downloaded on 5/24/2026 12:24:54 AM.
This article is licensed under a Creative Commons Attribution-NonCommercial 3.0 Unported Licence.

loadings (0.005 wt%), reaching values in the semiconductive range. Compared to previous WS_2-2D nanocomposites, which typically require higher loadings (above 1 wt%) and more complex processing routes, our approach preserves the 2D nature of WS_2 and achieves functional properties with minimal nanofiller content. Furthermore, our WS_2-2D nanosheets retain their excitonic emission post-printing, highlighting the advantages of this processing strategy for preserving intrinsic 2D material properties in 3D architectures. Overall, this work introduces a straightforward and versatile strategy to develop functional, 3D-printable nanocomposites with enhanced electrical and optical performance. By enabling the integration of such properties through a simple formulation approach, it opens new opportunities for advanced applications including ESD protection and tunable photonic or plasmonic devices.

Conflicts of interest

All authors have read and approved the final manuscript. The authors have no conflicts of interest to declare.

Data availability

The datasets generated and analyzed during the current study are available from the corresponding author on reasonable request.

Acknowledgements

Financial support of Junta de Andalucía under grant PROYEXCEL_00955, the Spanish Ministry of Science, Innovation, and Universities MICIU/AEI/10.13039/501100011033 (Project PID2023-151632OB-C22), FEDER-EU, and research group INNANOMAT (ref. TEP-946) is gratefully acknowledged. Authors acknowledge the use of instrumentation provided by the National Facility ELECMI ICTS, node División de Microscopía Electrónica (DME) at Universidad de Cádiz (UCA). Authors thank Rocío González Moya for the TGA measurements.

References

1 Y. Lei, T. Zhang, Y. C. Lin, T. Granzier-Nakajima, G. Bepete, D. A. Kowalczyk, Z. Lin, D. Zhou, T. F. Schranghamer, A. Dodda, A. Sebastian, Y. Chen, Y. Liu, G. Pourtois, T. J. Kempa, B. Schuler, M. T. Edmonds, S. Y. Quek, U. Wurstbauer, S. M. Wu, N. R. Glavin, S. Das, S. P. Dash, J. M. Redwing, J. A. Robinson and M. Terrones, Graphene and Beyond: Recent Advances in Two-Dimensional Materials Synthesis, Properties, and Devices, *ACS Nanosci. Au*, 2022, 450–485, DOI: 10.1021/acsnanoscienceau.2c00017.

2 M. Xu, T. Liang, M. Shi and H. Chen, Graphene-like Two-Dimensional Materials, *Chem. Rev.*, 2013, 3766–3798, DOI: 10.1021/cr300263a.

3 M. Chhowalla, H. S. Shin, G. Eda, L. J. Li, K. P. Loh and H. Zhang, The Chemistry of Two-Dimensional Layered Transition Metal Dichalcogenide Nanosheets, *Nat. Chem.*, 2013, 263–275, DOI: 10.1038/nchem.1589.

4 G. Zhou, J. Ji, Z. Chen, J. Shuai, Q. Liang and Q. Zhang, Scalable Electronic and Optoelectronic Devices Based on 2D TMDs, *Mater. Futures*, 2024, **3**, 042701, DOI: 10.1088/2752-5724/ad7c6c.

5 H. Huang, M. Zhang, K. Xu, Y. Zhuang, Y. Li and L. Wang, The Fundamentals, Progress, and Perspectives of Transition-Metal Dichalcogenides (TMDs) Applied in Advanced Oxidation Processes, *Chem. Eng. J.*, 2024, **484**, 149595, DOI: 10.1016/j.cej.2024.149595.

6 S. Aftab and H. H. Hegazy, Emerging Trends in 2D TMDs Photodetectors and Piezo-Phototronic Devices, *Small*, 2023, **19**(18), 2205778, DOI: 10.1002/smll.202205778.

7 H. Li, J. Wu, Z. Yin and H. Zhang, Preparation and Applications of Mechanically Exfoliated Single-Layer and Multilayer MoS2 and WSe2 Nanosheets, *Acc. Chem. Res.*, 2014, **47**(4), 1067–1075, DOI: 10.1021/ar4002312.

8 C. Lan, C. Li, J. C. Ho and Y. Liu, 2D WS2: From Vapor Phase Synthesis to Device Applications, *Adv. Electron. Mater.*, 2021, **7**(7), 2000688, DOI: 10.1002/aelm.202000688.

9 C. Li, D. Sang, S. Ge, L. Zou and Q. Wang, Recent Excellent Optoelectronic Applications Based on Two-Dimensional WS2 Nanomaterials: A Review, *Molecules*, 2024, **29**(14), 3341, DOI: 10.3390/molecules29143341.

10 S. G. Leonardi, W. Wlodarski, Y. Li, N. Donato, Z. Sofer, M. Pumera and G. Neri, A Highly Sensitive Room Temperature Humidity Sensor Based on 2D-WS2 Nanosheets, *FlatChem*, 2018, **9**, 21–26, DOI: 10.1016/j.flatc.2018.05.001.

11 C. Cong, J. Shang, Y. Wang and T. Yu, Optical Properties of 2D Semiconductor WS2, *Adv. Opt. Mater.*, 2018, **6**(1), 1700767, DOI: 10.1002/adom.201700767.

12 H. Tan, Y. Fan, Y. Zhou, Q. Chen, W. Xu and J. H. Warner, Ultrathin 2D Photodetectors Utilizing Chemical Vapor Deposition Grown WS2 with Graphene Electrodes, *ACS Nano*, 2016, **10**(8), 7866–7873, DOI: 10.1021/acsnano.6b03722.

13 A. Golbang, M. Mokhtari, E. Harkin-Jones, E. Archer and A. Mcilhagger, Additive Manufacturing and Injection Moulding of High-Performance IF-WS2/PEEK Nanocomposites: A Comparative Study, *Front. Mater.*, 2021, 8, DOI: 10.3389/fmats.2021.745088.

14 Y. Dai, X. H. Yan, X. Wu, D. W. Sha, M. Chen, H. Zou, J. Ren and X. N. Cheng, Facile Self-Assembly of AgNPs/WS2 Nanocomposites with Enhanced Electrochemical Properties, *Mater. Lett.*, 2016, **173**, 203–206, DOI: 10.1016/j.matlet.2016.03.050.

15 S. Shahabuddin, S. Mehmood, I. Ahmad and N. Sridewi, Synthesis and Characterization of 2D-WS2 Incorporated Polyaniline Nanocomposites as Photo Catalyst for Methylene Blue Degradation, *Nanomaterials*, 2022, **12**(12), 2090, DOI: 10.3390/nano12122090.

16 H. A. Colorado, E. I. Gutierrez-Velasquez, L. D. Gil and I. L. de Camargo, Exploring the Advantages and Applications of

© 2026 The Author(s). Published by the Royal Society of Chemistry

Open Access Article. Published on 06 March 2026. Downloaded on 5/24/2026 12:24:54 AM. This article is licensed under a Creative Commons Attribution-NonCommercial 3.0 Unported Licence.

Nanocomposites Produced via Vat Photopolymerization in Additive Manufacturing: A Review, *Adv. Compos. Hybrid Mater.*, 2024, **7**, 1, DOI: 10.1007/s42114-023-00808-z.

17 M. Aftab, S. Ikram, M. Ullah, N. Khan, M. Naeem, M. A. Khan, R. B. Bakhtiyor ogli, K. S. S. Qizi, O. O. Erkinjon Ugli, B. M. Abdurasulovna and O. K. A. Qizi, Recent Trends and Future Directions in 3D Printing of Biocompatible Polymers, *J. Manuf. Mater. Process.*, 2025, **9**(4), 129, DOI: 10.3390/jmmp9040129.

18 Y. Ma, C. Shih and Y. Bao, Advances in 4D Printing of Biodegradable Photopolymers, *Responsive Mater.*, 2024, **2**(3), e20240008, DOI: 10.1002/rpm.20240008.

19 M. Shah, A. Ullah, K. Azher, A. U. Rehman, W. Juan, N. Aktürk, C. S. Tüfekci and M. U. Salamci, Vat Photopolymerization-Based 3D Printing of Polymer Nanocomposites: Current Trends and Applications, *RSC Adv.*, 2023, 1456–1496, DOI: 10.1039/d2ra06522c.

20 Y. Li, W. Wang, F. Wu and R. K. Kankala, Vat Polymerization-Based 3D Printing of Nanocomposites: A Mini Review, *Front. Mater.*, 2023, **9**, 1118943, DOI: 10.3389/fmats.2022.1118943.

21 A. M. G. Cheadle, E. Maier, W. M. Palin, P. L. Tomson, G. Poologasundarampillai and M. A. Hadis, The Impact of Modifying 3D Printing Parameters on Mechanical Strength and Physical Properties in Vat Photopolymerisation, *Sci. Rep.*, 2025, **15**(1), 12592, DOI: 10.1038/s41598-025-97294-8.

22 N. Yosef Tal, H. Dodiuk, S. Farran, R. Carmieli, I. Pinkas, S. Kenig and R. Tenne, Accelerated Photocuring of Acrylate Resins with WS2 Nanoparticles, *ACS Appl. Polym. Mater.*, 2024, **6**(6), 3303–3315, DOI: 10.1021/acsapm.3c03119.

23 T. Di Luccio, C. Borriello, A. Bruno, M. G. Maglione, C. Minarini and G. Nenna, Preparation and Characterization of Novel Nanocomposites of WS2 Nanotubes and Polyfluorene Conductive Polymer, *Phys. Status Solidi A*, 2013, **210**(11), 2278–2283, DOI: 10.1002/pssa.201329333.

24 D. Bhattacharya, S. Bayan, R. K. Mitra and S. K. Ray, 2D WS2 Embedded PVDF Nanocomposites for Photosensitive Piezoelectric Nanogenerators with a Colossal Energy Conversion Efficiency of ~25.6%, *Nanoscale*, 2021, **13**(37), 15819–15829, DOI: 10.1039/D1NR03808G.

25 G. Mandal, R. B. Choudhary, B. A. Al-Asbahi and A. A. A. Ahmed, WS2 Incorporated PANI-RGO Nanocomposites Tailored for Inflated Thermal, Optical and Electrical Properties Used as ETL for OLEDs, *Opt. Mater.*, 2023, **146**, 114379, DOI: 10.1016/j.optmat.2023.114379.

26 F. I. Alzakia, W. Jonhson, J. Ding and S. C. Tan, Ultrafast Exfoliation of 2D Materials by Solvent Activation and One-Step Fabrication of All-2D-Material Photodetectors by Electrohydrodynamic Printing, *ACS Appl. Mater. Interfaces*, 2020, **12**(25), 28840–28851, DOI: 10.1021/acsami.0c06279.

27 W. Zhao, Z. Ghorannevis, L. Chu, M. Toh, C. Kloc, P. H. Tan and G. Eda, Evolution of Electronic Structure in Atomically Thin Sheets of Ws 2 and Wse2, *ACS Nano*, 2013, **7**(1), 791–797, DOI: 10.1021/nn305275h.

28 S. G. Prolongo, A. Jimenez-Suarez, R. Moriche and A. Ureña, In Situ Processing of Epoxy Composites Reinforced with Graphene Nanoplatelets, *Compos. Sci. Technol.*, 2013, **86**, 185–191, DOI: 10.1016/j.compscitech.2013.06.020.

29 A. S. De León and S. I. Molina, Influence of the Degree of Cure in the Bulk Properties of Graphite Nanoplatelets Nanocomposites Printed via Stereolithography, *Polymers*, 2020, **12**(5), 1103, DOI: 10.3390/polym12051103.

30 J. N. Coleman, M. Lotya, A. O'Neill, S. D. Bergin, P. J. King, U. Khan, K. Young, A. Gaucher, S. De, R. J. Smith, I. V. Shvets, S. K. Arora, G. Stanton, H. Y. Kim, K. Lee, G. T. Kim, G. S. Duesberg, T. Hallam, J. J. Boland, J. J. Wang, J. F. Donegan, J. C. Grunlan, G. Moriarty, A. Shmeliov, R. J. Nicholls, J. M. Perkins, E. M. Grieveson, K. Theuwissen, D. W. McComb, P. D. Nellist and V. Nicolosi, Two-Dimensional Nanosheets Produced by Liquid Exfoliation of Layered Materials, *Science*, 2011, **331**(6017), 568–571, DOI: 10.1126/science.1194975.

31 V. Vega-Mayoral, C. Backes, D. Hanlon, U. Khan, Z. Gholamvand, M. O'Brien, G. S. Duesberg, C. Gadermaier and J. N. Coleman, Photoluminescence from Liquid-Exfoliated WS2 Monomers in Poly(Vinyl Alcohol) Polymer Composites, *Adv. Funct. Mater.*, 2016, **26**(7), 1028–1039, DOI: 10.1002/adfm.201503863.

32 U. Khan, A. O'Neill, M. Lotya, S. De and J. N. Coleman, High-Concentration Solvent Exfoliation of Graphene, *Small*, 2010, **6**(7), 864–871, DOI: 10.1002/smll.200902066.

33 L. M. Valencia, M. Herrera, M. de la Mata, J. Hernández-Saz, I. Romero-Ocaña, F. J. Delgado, J. Benito and S. I. Molina, Stereolithography of Semiconductor Silver and Acrylic-Based Nanocomposites, *Polymers*, 2022, **14**(23), 5238, DOI: 10.3390/polym14235238.

34 M. Shah, A. Ullah, K. Azher, A. U. Rehman, W. Juan, N. Aktürk, C. S. Tüfekci and M. U. Salamci, Vat Photopolymerization-Based 3D Printing of Polymer Nanocomposites: Current Trends and Applications, *RSC Adv.*, 2023, **13**(2), 1456–1496, DOI: 10.1039/D2RA06522C.

35 X. L. X. Fu, A Low-Viscosity Flexible Photosensitive Resin for 3D Printing and Its Preparation Method and Application, Patent no CN113174016B, 2021.

36 A. Shastri, A. K. Das, S. Krishnakumar, P. J. Singh and B. N. Raja Sekhar, Spectroscopy of N,N-Dimethylformamide in the VUV and IR Regions: Experimental and Computational Studies, *J. Chem. Phys.*, 2017, **147**(22), 224305, DOI: 10.1063/1.5006126.

37 M. Maturi, L. Migliorini, S. M. Villa, T. Santaniello, N. Fernandez-Delgado, S. I. Molina, P. Milani, A. Sanz de León and M. C. Franchini, 3D-Printing of Highly Piezoelectric Barium Titanate Polymer Nanocomposites with Surface-Modified Nanoparticles at Low Loadings, *Adv. Funct. Mater.*, 2025, **35**(1), 2407077, DOI: 10.1002/adfm.202407077.

38 W. Zhao, Z. Ghorannevis, L. Chu, M. Toh, C. Kloc, P. H. Tan and G. Eda, Evolution of Electronic Structure in Atomically Thin Sheets of Ws 2 and Wse2, *ACS Nano*, 2013, **7**(1), 791–797, DOI: 10.1021/nn305275h.

39 Z. Li, F. Rashvand, H. Bretscher, B. M. Szydłowska, J. Xiao, C. Backes and A. Rao, Understanding the Photoluminescence

Open Access Article. Published on 06 March 2026. Downloaded on 5/24/2026 12:24:54 AM.
This article is licensed under a Creative Commons Attribution-NonCommercial 3.0 Unported Licence.

Quenching of Liquid Exfoliated WS2 Monolayers, *J. Phys. Chem. C*, 2022, **126**(51), 21681–21688, DOI: 10.1021/acs.jpcc.2c05284.

40 X. Wang, K. Kang, K. Godin, S. Fu, S. Chen and E.-H. Yang, Effects of Solvents and Polymer on Photoluminescence of Transferred WS2 Monolayers, *J. Vac. Sci. Technol., B: Nanotechnol. Microelectron.: Mater., Process., Meas., Phenom.*, 2019, **37**(5), 052902, DOI: 10.1116/1.5094543.

41 W. Di Cianni, M. de la Mata, F. J. Delgado, J. Hernández-Saz, M. Herrera, S. I. Molina, M. Giocondo and A. Sanz de León, Polymer Nanocomposites for Plasmonics: In Situ Synthesis of Gold Nanoparticles after Additive Manufacturing, *Polym. Test.*, 2023, **117**, 107869, DOI: 10.1016/j.polymertesting.2022.107869.

42 N. Peimyoo, J. Shang, C. Cong, X. Shen, X. Wu, E. K. L. Yeow and T. Yu, Nonblinking, Intense Two-Dimensional Light Emitter: Monolayer WS 2 Triangles, *ACS Nano*, 2013, **7**(12), 10985–10994, DOI: 10.1021/nn4046002.

43 M. Ahmadi, O. Zabihi, S. Jeon, M. Yoonessi, A. Dasari, S. Ramakrishna and M. Naebe, 2D Transition Metal Dichalcogenide Nanomaterials: Advances, Opportunities, and Challenges in Multi-Functional Polymer Nanocomposites, *J. Mater. Chem. A*, 2020, **8**(3), 845–883, DOI: 10.1039/C9TA10130F.

44 M. Kaur, K. Singh and A. Kumar, Trap States Induced Hopping Transport and Persistent Photoconductivity in WSe2/MoS2 Nanocomposite Thin Films, *J. Appl. Phys.*, 2021, **130**(12), 125308, DOI: 10.1063/5.0059381.

45 Y. Zare, N. Gharib, D.-H. Nam and Y.-W. Chang, Predicting of Tunneling Resistivity between Adjacent Nanosheets in Graphene–Polymer Systems, *Sci. Rep.*, 2023, **13**(1), 12455, DOI: 10.1038/s41598-023-39414-w.

46 Z. Hadi, J. K. Yeganeh, Y. Zare, M. Naqvi, K. Y. Rhee and S.-J. Park, Analysis of Tunneling Conductivity for MXene Polymer System by the Network of Interphase: Parametric Examinations and Experimental Validation, *Sci. Rep.*, 2025, **15**(1), 39616, DOI: 10.1038/s41598-025-23304-4.

© 2026 The Author(s). Published by the Royal Society of Chemistry